Zhang *et al. Energy Mater.* **2025**, *5*, 500063
DOI: 10.20517/energymater.2024.213

Energy Materials

Article

Open Access

Lithium-rich, oxygen-deficient spinel obtained through low-temperature decomposition of heterometallic molecular precursor

Yuxuan Zhang[1], Zheng Wei[1], Maria Batuk[2], Joke Hadermann[2], Alexander S. Filatov[3], Joyce Chang[1], Haixiang Han[4,*], Artem M. Abakumov[5,*], Evgeny V. Dikarev[1,*]

[1]Department of Chemistry, University at Albany, State University of New York, Albany, NY 12222, USA.
[2]EMAT, Department of Physics, University of Antwerp, Antwerp 2020, Belgium.
[3]Department of Chemistry, the University of Chicago, Chicago, IL 60637, USA.
[4]School of Material Science and Engineering, Tongji University, Shanghai 201804, China.
[5]Center for Energy Science and Technology, Skolkovo Institute of Science and Technology, Moscow 121205, Russia.

[*]**Correspondence to:** Prof. Evgeny V. Dikarev, Department of Chemistry, University at Albany, State University of New York, 1400 Washington Ave, Albany, NY 12222, USA. E-mail: edikarev@albany.edu; Prof. Artem M. Abakumov, Center for Energy Science and Technology, Skolkovo Institute of Science and Technology, Nobel Str. 3, Moscow 121205, Russia. E-mail: a.abakumov@skoltech.ru; Prof. Haixiang Han, School of Materials Science and Engineering, Tongji University, 4800 Cao'an Road, Shanghai 201804, China. E-mail: hxhan@tongji.edu.cn

How to cite this article: Zhang, Y.; Wei, Z.; Batuk, M.; Hadermann, J.; Filatov, A. S.; Chang, J.; Han, H.; Abakumov, A. M.; Dikarev, E. V. Lithium-rich, oxygen-deficient spinel obtained through low-temperature decomposition of heterometallic molecular precursor. *Energy Mater.* **2025**, *5*, 500063. https://dx.doi.org/10.20517/energymater.2024.213

Received: 14 Oct 2024 **First Decision:** 14 Nov 2024 **Revised:** 6 Dec 2024 **Accepted:** 20 Dec 2024 **Published:** 28 Feb 2025

Academic Editor: Yuhui Chen **Copy Editor:** Ping Zhang **Production Editor:** Ping Zhang

Abstract

A heterometallic single-source molecular precursor $Li_2Mn_2(tbaoac)_6$ (**1**, tbaoac = *tert*-butyl acetoacetato) has been specifically designed to achieve the lowest decomposition temperature and a clean conversion to mixed-metal oxides. The crystal structure of this tetranuclear molecule was determined by single crystal X-ray diffraction, and the retention of heterometallic structure in solution and in the gas phase was confirmed by nuclear magnetic resonance spectroscopy and mass spectrometry, respectively. Thermal decomposition of this precursor at the temperatures as low as 310 °C resulted in a new metastable oxide phase formulated as lithium-rich, oxygen-deficient spinel $Li_{1.5}Mn_{1.5}O_{3.5}$. This formulation was supported by a comprehensive suite of techniques including thermogravimetric/differential thermal analysis, elemental analysis, inductively coupled mass spectrometry, iodometric titration, X-ray photoelectron spectroscopy, high-resolution transmission electron microscopy studies, and Rietveld refinement from powder X-ray diffraction data. Upon heating to about 400 °C, this new low-temperature phase disproportionates stoichiometrically, gradually converting to layered Li_2MnO_3 and

© The Author(s) 2025. **Open Access** This article is licensed under a Creative Commons Attribution 4.0 International License (https://creativecommons.org/licenses/by/4.0/), which permits unrestricted use, sharing, adaptation, distribution and reproduction in any medium or format, for any purpose, even commercially, as long as you give appropriate credit to the original author(s) and the source, provide a link to the Creative Commons license, and indicate if changes were made.

spinel $Li_{1+x}Mn_{2-x}O_4$ ($x < 0.5$). Further heating to 750 °C results in formation of thermodynamically stable Li_2MnO_3 and $LiMn_2O_4$ phases.

Keywords: Heterometallic molecular precursor, thermal decomposition, lithium-manganese oxide, lithium-rich spinel, oxygen-deficient spinel

INTRODUCTION

Gaining access to kinetically metastable compounds is an important step toward the discovery of new functional materials having complementary or even superior properties to the known thermodynamically stable phases[1]. The intrinsic instability of such compounds often stems from their structural and compositional flexibilities that are sensitive to the external environment and build up the foundation for new interesting characteristics and reactivities[2]. The keys for those low-temperature/metastable phases are their constituent elements and chemical/coordination versatility[3].

Manganates are among the most promising classes of compounds for exploring new materials due to the unique position that manganese holds within the family of transition metals[4]. Manganates typically feature Mn in oxidation states of +3 or +4, often in varying ratios. The easy transition between Mn^{+3} and Mn^{+4} oxidation states can result in oxygen deficiency causing distorted coordination environments[5,6], while the Jahn-Teller effect, originating from the unique electronic configuration of Mn^{3+}, induces significant distortion in the [MnO_6] octahedra[7]. These two factors lead to a considerable variation in Mn-O bond lengths in manganates. Those distortions enhance the structural diversity of phases that are otherwise typically constructed with highly symmetric O_h octahedra[7,8]. Manganates are well-known for their diverse arrangements of octahedral building blocks, resulting in unique structures (such as tunnel structures) that are uncommon among other transition metals[9,10].

Incorporating a second metal into the manganate framework can further enhance its structural and compositional diversity, significantly broadening the potential applications of Mn-based materials[11,12]. Li^+ ions can occupy both tetrahedral and octahedral lattice sites introducing structural and compositional variations that are unknown for manganese neighbors on the Periodic Table[13,14]. These variations translate into a broad range of the Li:Mn ratios and different oxidation states for manganese from +3 ($LiMnO_2$) to mixed +3/+4 ($LiMn_2O_4$) to +4 (Li_2MnO_3 and $Li_4Mn_5O_{12}$). Structurally, these variations result in tertiary oxides with at least three distinct structure types: layered ($LiMnO_2$), spinel ($LiMn_2O_4$), and rock-salt ($Li_4Mn_2O_5$)[15-17].

It is not surprising that a number of unusual compounds in the Li-Mn-O system have been reported as metastable phases that exhibit unique properties[18]. For example, $Li_4Mn_2O_5$ with a rock-salt type structure was obtained through a room-temperature cation exchange approach[17]. This compound decomposes into thermodynamically stable phases such as $LiMnO_2$, Li_2O, and Li_2MnO_3 at elevated temperatures[19]. $Li_4Mn_2O_5$ has demonstrated a discharge capacity of 355 mAh/g as a positive electrode (cathode) in Li-ion batteries, which is the highest among all known lithium-transition metal oxides[17]. Another metastable phase, commonly referred to in literature as cubic spinel $Li_{1.6}Mn_{1.6}O_4$, was obtained at 350-450 °C by the calcination of orthorhombic $LiMnO_2$[20,21]. Upon further heating, the compound begins to decompose, as evidenced by the appearance of Li_2MnO_3[20]. This phase is currently under extensive investigation due to its very high Li^+ cation intercalation capacity. Some researchers believe that the above-mentioned compounds represent only a small fraction of the still untapped phases in the Li-Mn-O system[21,22].

Since the conventional high-temperature (> 500 °C) solid-state approaches are apparently not suitable for obtaining metastable phases, new synthetic strategies need to be explored. Those should be capable of affording fast, controllable kinetic routes that allow for the immediate formation of the metastable phase, and the whole preparation process should be mild enough in order to keep the operating temperatures below the decomposition point of the target compound. One viable approach is to employ heterometallic molecular precursors[23,24]. Within these molecular assemblies, the Li and Mn atoms are effectively set in a [-O-Li-O-Mn-O-] arrangement. Such pre-formed metal-oxygen bonds (oxo-bridges) and closely adjacent metal ions constitute prerequisites for the formation of unusual oxides through efficient kinetic pathways. Importantly, the organic O-containing ligands that bridge different metal atoms together play the most significant role in controlling low-temperature decomposition kinetics. We have previously found that $[Li_2M_2(tbaoac)_6]$ molecular precursors with the Li:M = 1:1 ratio and *tert*-butyl acetoacetato ligands are capable of producing lithium-transition metal oxides at the lowest decomposition temperatures[23,25]. Their thermal decomposition was reported to result in $LiFeO_2$, $LiCoO_2$, and $LiCo_{0.5}Ni_{0.5}O_2$ layered phases. However, thermal decomposition of the corresponding Mn precursor is unlikely to result in layered $LiMnO_2$, since the latter can only be obtained in oxygen-depleted processes. At the same time, the 1:1 metal ratio is at the crossroads of different structure types in the Li-Mn-O system from layered oxides $LiMnO_2$ to Li insertion into $Li_4Mn_5O_{12}$ spinel to Li de-intercalation from $Li_4Mn_2O_5$ rock salt.

In this work, we present evidence for a new metastable Li manganate, formulated as lithium-rich, oxygen-deficient spinel-type $Li_{1.5}Mn_{1.5}O_{3.5}$ with mixed-valent $Mn^{+3/+4}$ ions. This compound was obtained through the thermal decomposition of single-source molecular precursor $[Li_2Mn_2(tbaoac)_6]$ in the air at approximately 300 °C. We show that, upon further heating, this phase disproportionates stoichiometrically into the thermodynamically stable $Li_2Mn^{IV}O_3$ and $LiMn^{III/IV}{}_2O_4$.

EXPERIMENTAL

Materials

Anhydrous manganese(II) chloride ($MnCl_2$) and lithium methoxide (LiOMe) were purchased from Sigma-Aldrich and used as received after verifying their X-ray powder diffraction patterns. *Tert*-butyl acetoacetate (Htbaoac) was purchased from Sigma-Aldrich and used as received after confirming its ^{1}H nuclear magnetic resonance (NMR) spectrum. Li(tbaoac) was prepared according to the literature synthesis procedure[26].

Preparation of $Li_2Mn_2(tbaoac)_6$ (1)

Li(tbaoac) (0.391 g, 2.38 mmol) and $MnCl_2$ (0.100 g, 0.794 mmol) were added to a 100 mL flask under argon atmosphere, followed by the addition of 40 mL of dry ethanol. The resulting colorless solution was stirred at room temperature for one hour. The solvent was then evaporated under vacuum at room temperature and the white solid residue was further dried overnight at 100 °C. The final white product was isolated by dichloromethane extraction followed by evaporation of the solvent at room temperature, yielding approximately 0.400 g (95 %). The purity of the bulk crystalline product was confirmed by X-ray powder diffraction [Supplementary Figure 1 and Supplementary Table 1].

Characterization

Le Bail fit for X-ray powder diffraction patterns was performed using the TOPAS version 4 software package (Bruker AXS, 2006). The attenuated total reflection (ATR) spectra were recorded on a PerkinElmer Spectrum 100FT-IR spectrometer. NMR spectra were collected using a Bruker Avance 400 spectrometer at 400 MHz for ^{1}H and at 155.5 MHz for ^{7}Li. Chemical shifts (δ) are given in ppm relative to the residual solvent peaks for ^{1}H, and to ^{7}Li peak of external standard (0.1 M solution of LiCl in D_2O). Mass spectra were acquired using a Direct Analysis in Real Time -Standardized Voltage and Pressure (DART-SVP) ion source

(IonSense, Saugus, MA, USA) coupled to a JEOL AccuTOF time-of-flight mass spectrometer (JEOL USA, Peabody, MA, USA) in positive ion mode. Spectra were recorded over the mass range of m/z 200-2000 at one spectrum per second with a gas heater set at 350 °C. Thermal decomposition of heterometallic precursors was performed in air at ambient pressure. Approximately 40 mg of the solid sample was placed into a 20 mL Coors high-alumina crucible (Aldrich) and heated at a rate of approximately 35 °C/min in a muffle furnace (Lindberg Blue M). The decomposition residues were analyzed using X-ray powder diffraction. X-ray powder diffraction data were collected on a Bruker D8 Advance diffractometer (Cu K_α radiation, focusing Göbel Mirror, LynxEye one-dimensional detector, step of 0.02° 2θ, 20 °C). Metal ratios were determined using inductively coupled plasma (ICP) analysis conducted on a Perkin-Elmer Optima 3300 DV ICP instrument. X-ray photoelectron spectroscopy (XPS) was performed on a Kratos Axis Nova spectrometer with a monochromatic Al K_α source ($h\nu$ = 1486.6 eV). The Al anode was operated at 10 mA and 15 kV. The instrument work function was calibrated to give an Au $4f_{7/2}$ metallic gold binding energy (BE) of 83.95 eV. The spectra were calibrated to the C 1*s* peak of adventitious carbon at 284.8 eV. The base pressure of the instrument was 1 × 10^{-9} Torr. The spectra covering Mn $2p_{1/2}/2p_{3/2}$, O 1*s* and C 1*s* area were collected using an analysis area of 0.3 × 0.7 mm^2, with a pass energy of 80 eV, and a step size of 0.5 eV. The etching was performed using an Ar^+ ion gun operated at 2 keV, with a raster size of 3 × 3 mm^2 and a current density of about 31 μA/cm^2. Electron diffraction (ED) patterns, transmission electron microscopy (TEM) images, high angle annular dark field scanning TEM (HAADF-STEM) images and energy dispersive X-ray (EDX) spectra were obtained using a FEI Osiris transmission electron microscope operated at 200 kV and equipped with a Super-X EDX system. TEM specimens were prepared by grinding the powder in a mortar in anhydrous ethanol and depositing drops of the suspension onto holey carbon grids.

RESULTS AND DISCUSSION

Synthesis and characterization of heterometallic precursor 1

The heterometallic precursor complex $[Li_2Mn_2(tbaoac)_6]$ (**1**) was obtained by a simple solution reaction procedure that employs commercially/readily available starting reagents on a large scale with nearly quantitative yield:

$$6Li(tbaoac) + 2MnCl_2 \rightarrow Li_2Mn_2(tbaoac)_6 + 4LiCl \quad (1)$$

This reaction represents an interaction of anhydrous manganese(II) chloride with an excess of unsolvated Li(tbaoac) salt. The heterometallic complex can be readily separated from LiCl byproduct based on their different solubilities in dichloromethane. The isolated precursor **1** appears as a white powder that is relatively stable in the open air and can be handled outside of the glove box for a reasonable period of time in the course of characterization and decomposition studies. Precursor **1** was found to be quantitatively resublimed at 160 °C under dynamic vacuum conditions and can be further purified by sublimation at temperatures below its decomposition point (*ca.* 185 °C). Precursor **1** is instantly soluble in a variety of common solvents.

Single crystal X-ray diffraction analysis revealed that precursor **1** consists of tetranuclear heterocyclic molecules $[Li_2Mn_2(tbaoac)_6]$ [Figure 1], similar to those of other transition metals (Fe[23], Co[26], and Ni[25]). All crystals of precursor **1** were found to be allotwins[26] consisting of an intergrowth of two polymorphs (triclinic and monoclinic), regardless of the crystal size or growth conditions. A satisfactory Le Bail fit for the experimental X-ray powder diffraction pattern of bulk product **1** was obtained by comparing it with the one calculated for the mixture of two modifications: the major triclinic and the minor monoclinic phases [Supplementary Figure 1 and Supplementary Table 1].

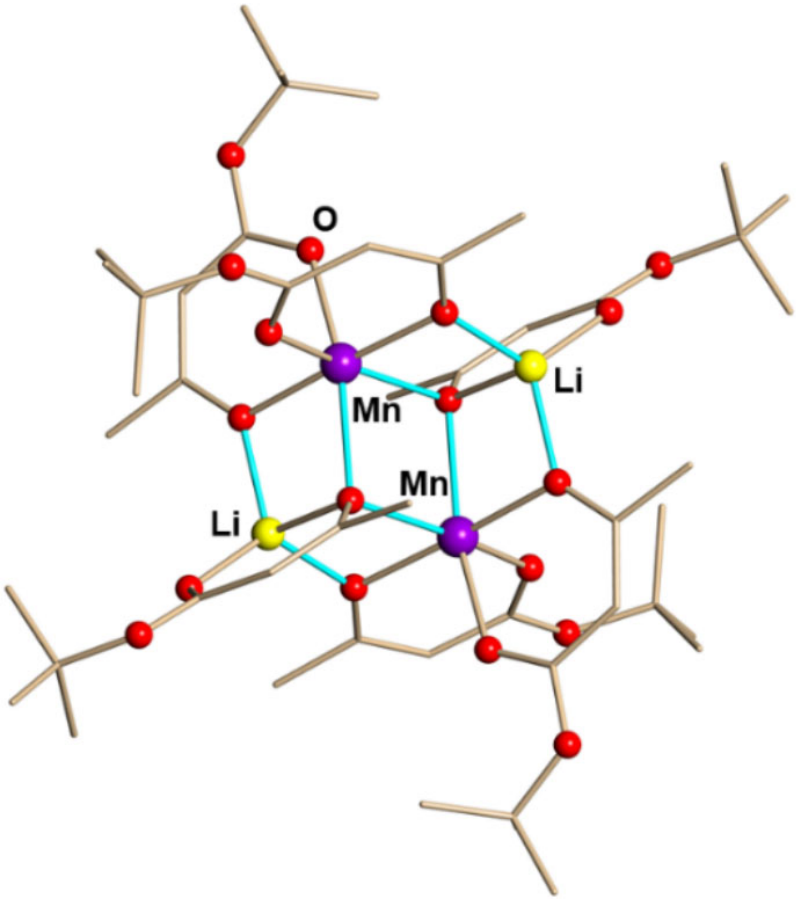

Figure 1. Solid state structure of heterometallic molecular precursor $[Li_2Mn_2(tbaoac)_6]$ (**1**). Bridging M-O (M = Li, Mn) bonds are highlighted in blue. Hydrogen atoms are omitted for clarity. Single crystal growth of precursor **1** is shown in Supplementary Table 2. Detailed views of molecular structure **1**, including thermal ellipsoids, are available in Supplementary Figure 2. Unit cell parameters, selected bond distances and angles of precursor **1** are recorded in Supplementary Tables 3 and 4.

The ATR spectrum of precursor **1** was measured and shown in Supplementary Figure 3. The ^{1}H and ^{7}Li NMR spectra of complex **1** in deuterated chloroform, acetone, and tetrahydrofuran (THF) [Supplementary Figures 4 and 5] are all silent, indicating that the heterometallic structure is retained in these organic solvents. The gas phase structure of the heterometallic precursor was investigated by direct analysis in real time (DART) mass spectrometry[27]. This analysis [Figure 2] revealed the presence of the heterometallic tetranuclear species $[M\text{-}L]^+$ {M = $[Li_2Mn_2(tbaoac)_6]$, L = tbaoac} with characteristic isotope distribution pattern in the gas phase. The complete assignment of the ions detected in the spectrum is provided in the Supplementary Figure 6, Supplementary Tables 5 and 6.

Low-temperature decomposition oxide product

Heterometallic precursors similar to **1** have been reported[23,25,26] to yield crystalline lithium-transition metal oxides $LiMO_2$ (M = Fe, Co, Co/Ni) with a Li:M ratio of 1:1 upon thermal decomposition at temperatures as low as 280 °C. Thermogravimetric analysis (TGA) of heterometallic precursor **1** shows that the thermal decomposition process is quite complex and is mostly complete by 310 °C [Figure 3]. Lower decomposition temperature (280 °C) would lead to the appearance of impurities [Supplementary Figure 7]. The isotherm recorded at 310 °C reveals residue weight stabilizes after 24 h. The X-ray powder diffraction pattern indicates that phase-pure material is obtained after the decomposition at 310 °C [Figure 4].

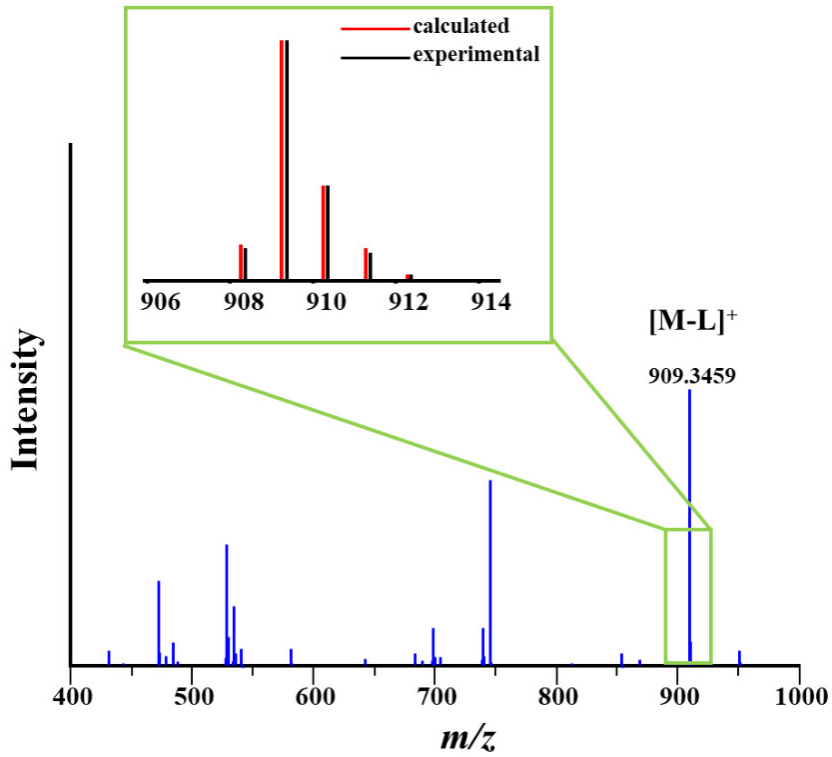

Figure 2. Positive-ion DART mass spectrum of solid $[Li_2Mn_2(tbaoac)_6]$ (**1**). The isotope distribution pattern for the $[M\text{-}L]^+$ {M = $[Li_2Mn_2(tbaoac)_6]$, L = tbaoac} ion is inset. DART: Direct analysis in real time.

The Le Bail fit of the X-ray powder diffraction pattern revealed the cubic crystal system with a unit cell parameter of a = 8.1170(1) Å [Figure 4], which is smaller than those (8.221 - 8.162 Å) for any reported Li-Mn spinel phases $Li_{1+x}Mn_{2-x}O_4$ (x = 0 - 0.33)[20,28-31]. The smaller unit cell parameter can be attributed to the increased lithium content and/or decreased oxygen content in the spinel structure.

The low-temperature phase obtained from the thermal decomposition of the molecular precursor was investigated using ED and high-resolution TEM (HRTEM). Overview TEM images are shown in the Supplementary Figure 8. The phase consists of highly agglomerated crystallites ranging in size from a few nanometers up to approximately 60 nm. An ED ring pattern measured from a group of crystallites is shown in Figure 5A. It can be completely indexed in a cubic *Fd*-3*m* lattice with unit cell parameter a≈8.0 Å. The intensity profile was measured from this pattern. Figure 5B represents the Le Bail fit of the profiled ED data. The refined cell parameter was found to be a = 7.98(2) Å.

Electron nanodiffraction patterns taken along the [001], [-110], and [-112] zone axes of the spinel-type face-centered lattice are shown in Figure 5C-E. The following reflection conditions were derived from these images: *hkl*: $h + k = 2n$, $h + l = 2n$, $k + l = 2n$ and 0*kl*: $k + l = 4n$, $k = 2n$, $l = 2n$. These reflection conditions indicate the *Fd*-3*m* (or *Fd*-3) space group. The 00*l* reflections with $l = 2n$ observed on the [-112] diffraction pattern are due to double diffraction. HRTEM images from several crystallites and their corresponding fast Fourier transforms (FFT) are given in Figure 5F-H. The FFTs are consistent with the electron nanodiffraction patterns in Figure 5C-E.

Since the conventional high-temperature (> 500 °C) solid-state approaches are apparently not suitable for obtaining metastable phases, new synthetic strategies need to be explored. Those should be capable of affording fast, controllable kinetic routes that allow for the immediate formation of the metastable phase, and the whole preparation process should be mild enough in order to keep the operating temperatures below the decomposition point of the target compound. One viable approach is to employ heterometallic molecular precursors[23,24]. Within these molecular assemblies, the Li and Mn atoms are effectively set in a [-O-Li-O-Mn-O-] arrangement. Such pre-formed metal-oxygen bonds (oxo-bridges) and closely adjacent metal ions constitute prerequisites for the formation of unusual oxides through efficient kinetic pathways. Importantly, the organic O-containing ligands that bridge different metal atoms together play the most significant role in controlling low-temperature decomposition kinetics. We have previously found that $[Li_2M_2(tbaoac)_6]$ molecular precursors with the Li:M = 1:1 ratio and *tert*-butyl acetoacetato ligands are capable of producing lithium-transition metal oxides at the lowest decomposition temperatures[23,25]. Their thermal decomposition was reported to result in $LiFeO_2$, $LiCoO_2$, and $LiCo_{0.5}Ni_{0.5}O_2$ layered phases. However, thermal decomposition of the corresponding Mn precursor is unlikely to result in layered $LiMnO_2$, since the latter can only be obtained in oxygen-depleted processes. At the same time, the 1:1 metal ratio is at the crossroads of different structure types in the Li-Mn-O system from layered oxides $LiMnO_2$ to Li insertion into $Li_4Mn_5O_{12}$ spinel to Li de-intercalation from $Li_4Mn_2O_5$ rock salt.

In this work, we present evidence for a new metastable Li manganate, formulated as lithium-rich, oxygen-deficient spinel-type $Li_{1.5}Mn_{1.5}O_{3.5}$ with mixed-valent $Mn^{+3/+4}$ ions. This compound was obtained through the thermal decomposition of single-source molecular precursor $[Li_2Mn_2(tbaoac)_6]$ in the air at approximately 300 °C. We show that, upon further heating, this phase disproportionates stoichiometrically into the thermodynamically stable $Li_2Mn^{IV}O_3$ and $LiMn^{III/IV}{}_2O_4$.

EXPERIMENTAL

Materials

Anhydrous manganese(II) chloride ($MnCl_2$) and lithium methoxide (LiOMe) were purchased from Sigma-Aldrich and used as received after verifying their X-ray powder diffraction patterns. *Tert*-butyl acetoacetate (Htbaoac) was purchased from Sigma-Aldrich and used as received after confirming its ^{1}H nuclear magnetic resonance (NMR) spectrum. Li(tbaoac) was prepared according to the literature synthesis procedure[26].

Preparation of $Li_2Mn_2(tbaoac)_6$ (1)

Li(tbaoac) (0.391 g, 2.38 mmol) and $MnCl_2$ (0.100 g, 0.794 mmol) were added to a 100 mL flask under argon atmosphere, followed by the addition of 40 mL of dry ethanol. The resulting colorless solution was stirred at room temperature for one hour. The solvent was then evaporated under vacuum at room temperature and the white solid residue was further dried overnight at 100 °C. The final white product was isolated by dichloromethane extraction followed by evaporation of the solvent at room temperature, yielding approximately 0.400 g (95 %). The purity of the bulk crystalline product was confirmed by X-ray powder diffraction [Supplementary Figure 1 and Supplementary Table 1].

Characterization

Le Bail fit for X-ray powder diffraction patterns was performed using the TOPAS version 4 software package (Bruker AXS, 2006). The attenuated total reflection (ATR) spectra were recorded on a PerkinElmer Spectrum 100FT-IR spectrometer. NMR spectra were collected using a Bruker Advance 400 spectrometer at 400 MHz for ^{1}H and at 155.5 MHz for ^{7}Li. Chemical shifts (δ) are given in ppm relative to the residual solvent peaks for ^{1}H, and to ^{7}Li peak of external standard (0.1 M solution of LiCl in D_2O). Mass spectra were acquired using a Direct Analysis in Real Time -Standardized Voltage and Pressure (DART-SVP) ion source

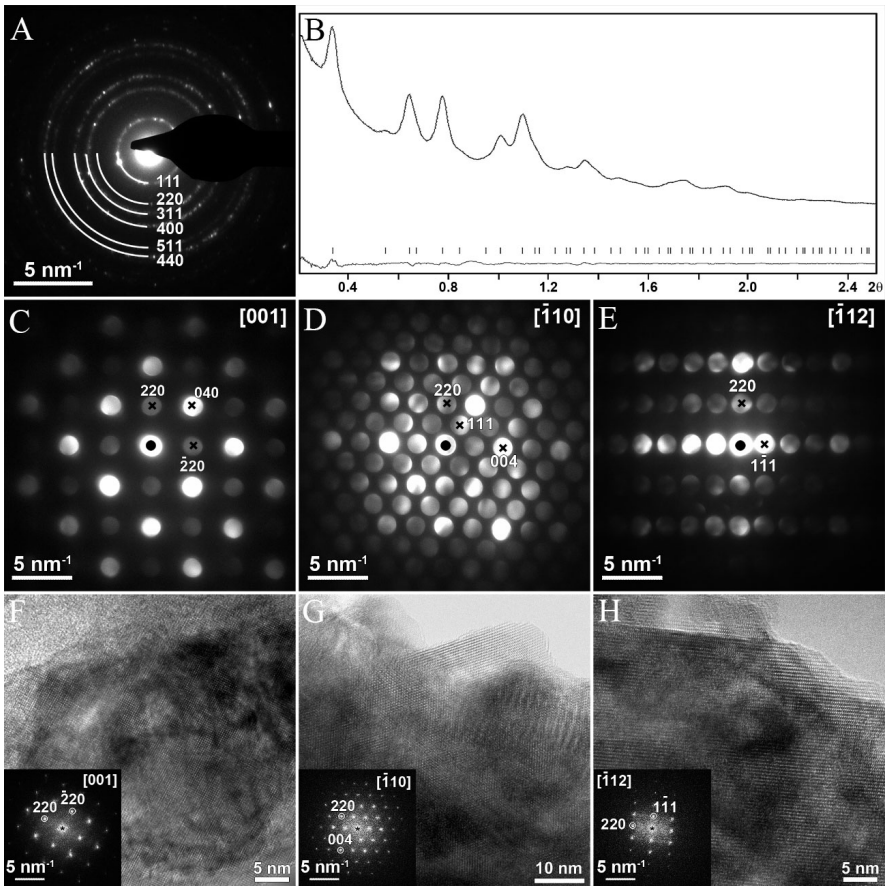

Figure 5. (A) Electron diffraction ring pattern and (B) the corresponding intensity profile measured from the electron diffraction ring pattern, the tick marks represent the Le Bail fit; (C-E) electron nanodiffraction patterns of $Li_{1.5}Mn_{1.5}O_{3.5}$; (F-H) HRTEM images and corresponding fast Fourier transforms (FFT) taken from different crystallites of $Li_{1.5}Mn_{1.5}O_{3.5}$. HRTEM: High-resolution transmission electron microscopy.

The spinel structure model was applied for the Rietveld refinement using the powder X-ray diffraction (XRD) pattern. The cation and oxygen positions were refined with the same thermal parameter. Occupancy factors for the tetrahedral and octahedral metal sites were refined assuming the full occupancy of the tetrahedral site by Li cations and joint occupancy of the octahedral site by Li and Mn ions in the ~0.25:0.75 ratio. Very good agreement between the experimental and calculated XRD profiles has been achieved after the refinement [Figure 6]. The structure parameters and reliability factors are summarized in Table 1. Based on all the above results, the new oxide phase was formulated as lithium-rich, oxygen-deficient spinel $Li_{1.5}Mn_{1.5}O_{3.5}$.

High-temperature decomposition products

TGA of the $Li_{1.5}Mn_{1.5}O_{3.5}$ oxide obtained at 310 °C shows almost no weight loss until 600 °C [Figure 7], but two significant features are observed. First, a strong endothermal signal is present in the Differential thermal analysis (DTA) curve between 475 °C and 600 °C [Figure 7]. Second, X-ray powder diffraction reveals the appearance of additional peaks at around 400 °C [Figure 8]. These observations suggest that a stoichiometric transformation or disproportionation is occurring without the release of any volatiles. Continued temperature increase leads to a new phase, identified as monoclinic Li_2MnO_3, accompanied by its characteristic red color in the solid samples. Additionally, the unit cell parameter of the spinel phase gradually increases, indicating a transformation of $Li_{1+x}Mn_{2-x}O_{4-\delta}$ towards a spinel structure with lower

Table 1. Crystallographic data for $Li_{1.494}Mn_{1.506}O_{3.5}$ obtained by the Rietveld refinement

Formula			$Li_{1.494}Mn_{1.506}O_{3.5}$		
Space group	*Fd*-3*m*				
Z	8				
a, Å	8.1398(6)				
Position	Occupancy	*x*/*a*	*y*/*b*	*z*/*c*	U_{iso}, Å^2
Li1	1	1/8	1/8	1/8	0.0236(3)
Mn1	0.753(8)	1/2	½	1/2	0.0236(3)
Li2	0.247(8)	1/2	½	1/2	0.0236(3)
O1	0.875(3)	0.2567(4)	0.2567(4)	0.2567(4)	0.0236(3)

d (Li1–O1) = 1.8571(21) Å (4x); *d* (Mn1–O1) = 1.9820(11) Å (6x); R_1 = 0.032; R_p = 0.040; R_{wp} = 0.030.

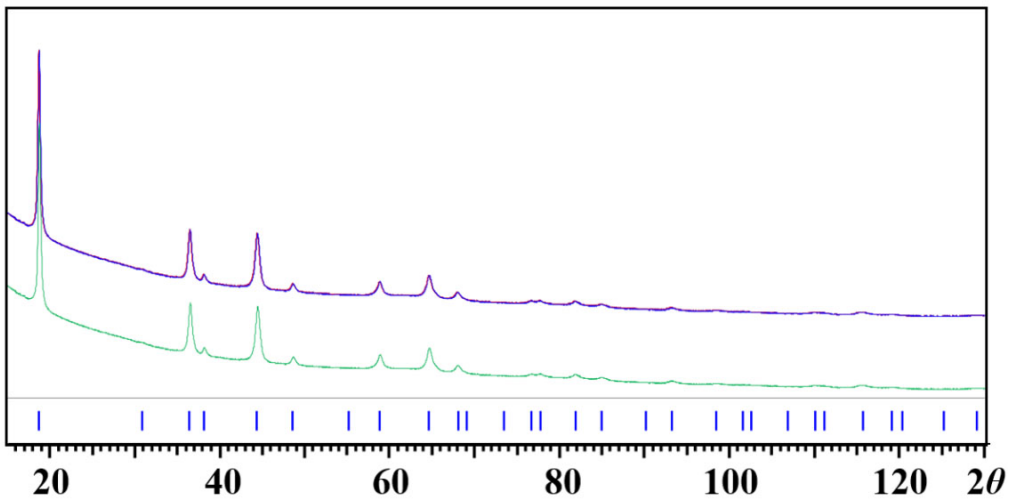

Figure 6. Experimental, calculated and difference Rietveld profiles after the refinement of the $Li_{1.494}Mn_{1.506}O_{3.5}$ structure. The red and blue curves are the overlaid experimental and calculated patterns. The green curve is the calculated pattern. The grey line is the difference curve. Theoretical peak positions are shown at the bottom.

lithium/higher oxygen content to compensate for the formation of lithium-rich Li_2MnO_3.

At 600 °C, the X-ray powder diffraction pattern clearly reveals the presence of two distinct phases [Figures 8 and 9A]: Li_2MnO_3 and $LiMn_2O_4$. The main phase can be indexed using a monoclinic *C*-centered lattice with unit cell parameters a = 4.9298(4) Å, b = 8.5276(6) Å, c = 5.0223(4) Å, β = 109.333(5)° [Supplementary Figure 10 and Supplementary Table 7], consistent with a Li_2MnO_3-type structure. However, the Li_2MnO_3 phase alone does not allow adequate fitting of the powder X-ray diffraction pattern [Supplementary Figure 11]. A reasonable fit was achieved only when an *F*-centered cubic spinel-type phase with a = 8.1524(5) Å was included in the refinement [Supplementary Figure 12].

HAADF-STEM images revealed that the sample contains two distinct types of crystals differing in size and shape [Figure 9B]. The larger crystals are octahedral in shape and range in size from 50 nm to 300 nm, while the smaller crystals, measuring 5 nm to 50 nm, do not exhibit well-defined facets. Although the two types of crystals are closely intermixed, it was possible to obtain ring ED patterns from areas with a preferential abundance of either small or large crystals [Figure 9C]. The intensity profiles integrated around the rings are shown in Figure 9D. The ring ED pattern of the small crystals displays an intensity distribution similar to

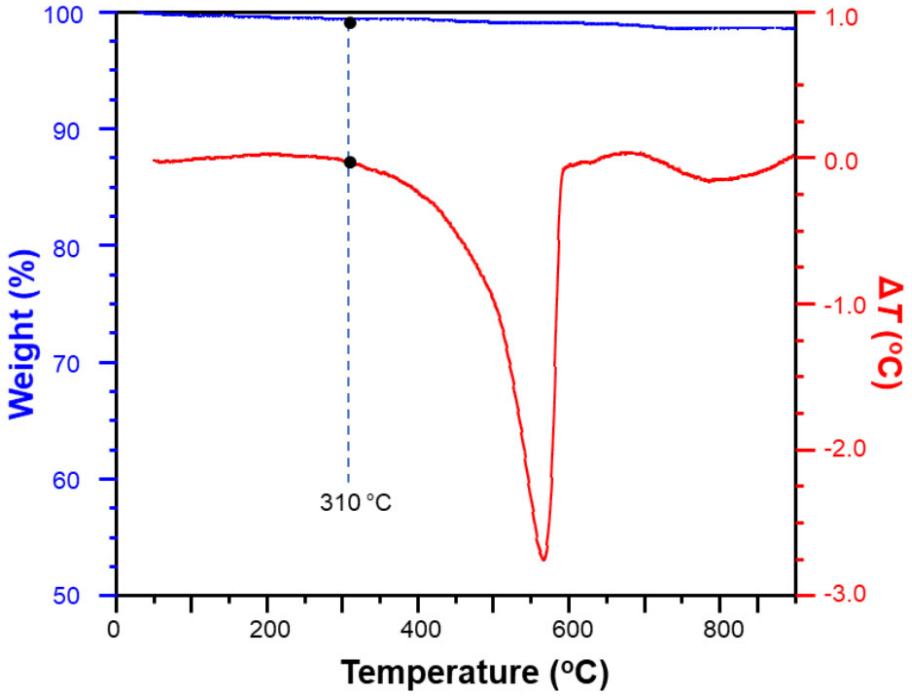

Figure 7. TGA (blue) and DTA (red) curves of $Li_{1.5}Mn_{1.5}O_{3.5}$ obtained at 310 °C. Δ*T* represents the temperature difference between the sample and reference. TGA: Thermogravimetric analysis; DTA: differential thermal analysis.

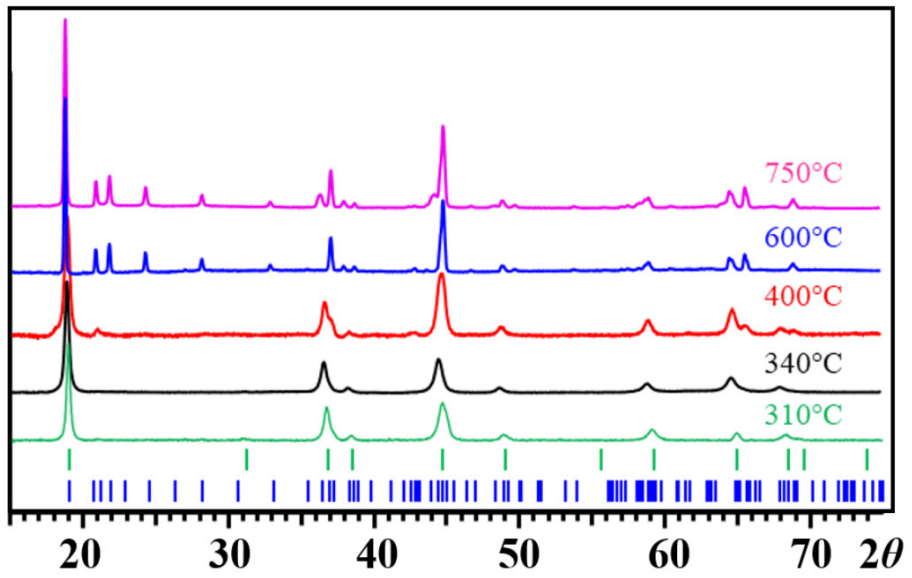

Figure 8. Powder X-ray diffraction patterns of the residues obtained by decomposition of heterometallic precursor **1** at different temperatures. Theoretical peak positions shown at the bottom represent the spinel phase (green) and Li_2MnO_3 (blue).

that expected for the spinel $LiMn_2O_4$ phase. The shoulder at the 111 spinel reflection is attributed to the simultaneous presence of the Li_2MnO_3 phase, in which these reflections originate from the Li and Mn "honeycomb" ordering in the $LiMn_2$ layers. The ring ED pattern from the large crystals corresponds to the Li_2MnO_3 phase (Figure 9E, top) considering a preferred orientation correction (March-Dollase parameter of 1.4 along the [001] direction) (Figure 9E, bottom). This is typical for large, anisotropic crystals deposited

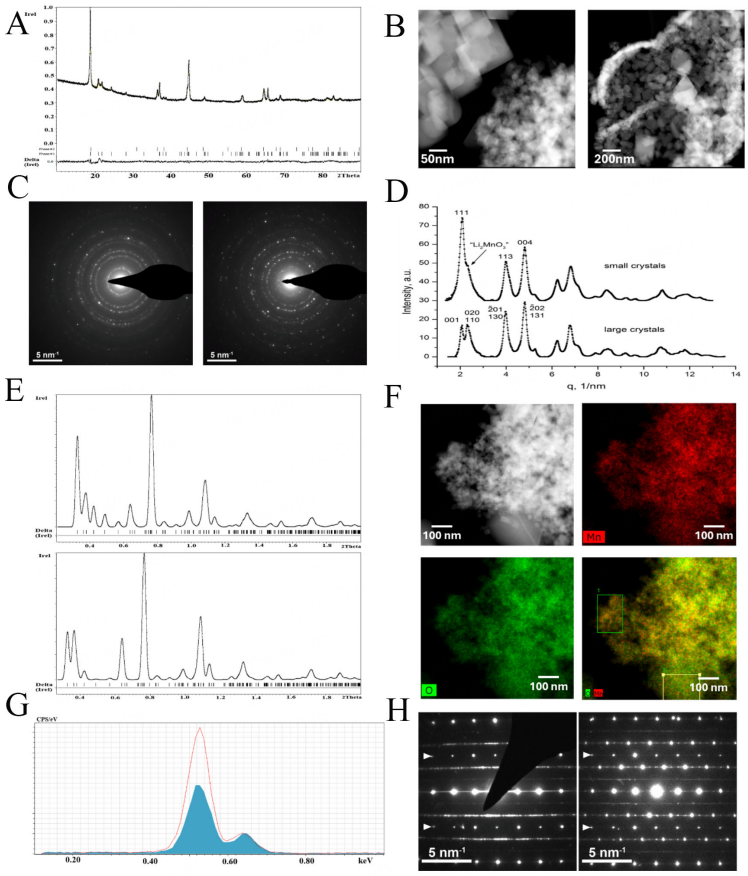

Figure 9. (A) Fit of the powder X-ray diffraction pattern of the sample obtained by the thermal decomposition of $Li_{1.5}Mn_{1.5}O_{3.5}$ at 600 °C with a mixture of Li_2MnO_3 and $LiMn_2O_4$ phases; (B) HAADF-STEM images of the nanocrystalline phases in the sample obtained by the thermal decomposition of $Li_{1.5}Mn_{1.5}O_{3.5}$ at 600 °C; (C) Ring electron diffraction patterns of the small (left) and large crystals (right) in phase (B); (D) Intensity profiles of the ring ED patterns indexed with the spinel *F*-centered cubic cell (top) and the Li_2MnO_3 *C*-centered monoclinic unit cell (bottom); (E) Theoretical electron diffraction pattern of the Li_2MnO_3 phase (top) and the theoretical electron diffraction pattern of the Li_2MnO_3 phase affected by preferred orientation; (F) HAADF-STEM image, Mn and O EDX signal maps and a mixed colored map; (G) EDX spectra at the O-K_α and Mn-L_α lines indicating that the large Li_2MnO_3 crystal (area 2 in the panel F) has a higher O-content (red spectrum). The spectrum of the area of small $LiMn_2O_4$ crystals (area 1, blue spectrum) demonstrates a clearly lower intensity of the O-*K* line compared to that of the large Li_2MnO_3 crystals (red); (H) ED patterns of the Li_2MnO_3 phase. The reflections due to spinel intergrowth are marked with arrows. HAADF-STEM: High angle annular dark field scanning transmission electron microscopy; ED: Electron diffraction; EDX: Energy dispersive X-ray.

onto a flat surface such as the carbon support. It should be noted that the intensities are also affected by the simultaneously present spinel phase.

Although the exact quantification of the Mn to O ratio using EDX spectra is impossible, this ratio can be qualitatively estimated from the relative intensities of the O-K_α (at 525 eV) and Mn-L_α (at 637 eV) lines, which are close in energy and, hence, their ratio is not strongly affected by absorption due to variations in crystal thickness. EDX analysis of the residue revealed a highly homogeneous distribution of manganese and oxygen [Figure 9F]. The oxygen content in the Li_2MnO_3-like large crystals is clearly higher than that in the small spinel-like crystals [Figure 9G]. Additional HAADF-STEM images of different crystals can be found in the Supplementary Figure 13. Besides existing as separate crystallites, the Li_2MnO_3 and spinel phases also form intergrowths, as indicated by the extra reflections, marked with arrows in Figure 9H, in the ED patterns of Li_2MnO_3, which are attributed to the spinel phase[32].

High-temperature treatment (750 °C) of $Li_{1.5}Mn_{1.5}O_{3.5}$ resulted in a mixture of Li_2MnO_3 and $LiMn_2O_4$ (Equation 2) as confirmed by X-ray powder diffraction [Figure 10]. The unit cell parameters of Li_2MnO_3 and $LiMn_2O_4$ obtained from the Le Bail fit correspond well with the values reported in the literature [Table 2].

$$2Li_{1.5}Mn_{1.5}O_{3.5} \rightarrow Li_2MnO_3 + LiMn_2O_4 \quad (2)$$

From a crystal chemistry point of view, the metastable nature of the $Li_{1.5}Mn_{1.5}O_{3.5}$ spinel phase is not surprising considering mixed Mn valence of +3.67, incomplete coordination environment for both cations due to oxygen vacancies and mixed occupancy of the 16*d* crystallographic site with the Mn^{3+}, Mn^{4+} and Li^+ cations with quite different ionic radii: $r(Mn^{3+})$ = 0.645 Å, $r(Mn^{4+})$ = 0.53 Å, and $r(Li^+)$ = 0.76 Å. No wonder that it tends to be thermally decomposed upon exsolving Li_2MnO_3 with a very strong Mn^{4+}-O bond, complete octahedral oxygen coordination around the Mn^{4+} cations and robust "honeycomb" Li/Mn cation ordering accommodating the size and charge differences. This can be considered as the main driving force behind the phase transition under discussion.

The mechanism of transformation of the Li-rich spinel structures into the Li_2MnO_3-type structures has already been discussed in the literature. According to the experimental and theoretical study by Pei *et al.*[35], the transformation occurs through a migration of the tetrahedrally-coordinated Li at the 8a crystallographic site to the octahedral 16c site that creates a fragment of the Li_2MnO_3-type layered structure. It should be noted that in the original work of Pei *et al.*[35], this cation migration is facilitated by oxygen vacancies generated due to O_2 release upon heating of their Li-rich spinel. The reported $Li_{1.5}Mn_{1.5}O_{3.5}$ spinel phase does not need oxygen release to create vacancies as they are already present in this anion-deficient composition. This makes the mechanism discussed above highly plausible in this case.

Historical perspective

We strongly believe that all tertiary oxides, particularly those in well-studied systems such as Li-Mn-O, [Supplementary Table 8] have likely been detected or reported before. The real question is how such a "new" phase was formulated and on which methods or characteristics this assignment was based. Many unusual phases have been reported in the Li-Mn-O system[17,33,36]. From our extensive search of the literature, the phase most similar to the one we report here was recorded back in 1996[37]. It was obtained by calcination in the air of the *o*-$LiMnO_2$ modification (which itself was synthesized hydrothermally at 160-220 °C) between 300 °C and 400 °C for 24 h. This phase was identified as cubic spinel with the unit cell parameter of 8.14 Å. The authors formulated it as $Li_{0.99}MnO_{2.32-2.39}$ ($Li_{1.492}Mn_{1.508}O_{3.50-3.60}$ in "spinel terms") with an average manganese valency of +3.6 to +3.8. The Li content was determined by atomic absorption spectroscopy, the Mn oxidation state was derived from chemical titration, and the oxygen content was calculated based on both Li content and Mn oxidation state. The authors also reported that the new phase oxidizes further in air if heated above 400 °C, decomposing into a mixture of Li_2MnO_3 and $LiMn_2O_4$.

CONCLUSIONS

Compounds with low thermal stability that cannot withstand traditional synthetic methods often remain undiscovered due to the limited variety of low-temperature synthetic routes available. Mixed-metal manganates are prime candidates for revealing new metastable phases that can be accessed using soft-chemistry approaches at low temperatures. The Li-Mn-O system, in particular, still holds potential for new discoveries, despite extensive investigation over the years.

Table 2. Comparison of the unit cell parameters for Li_2MnO_3 and $LiMn_2O_4$ oxides obtained by heating of $Li_{1.5}Mn_{1.5}O_{3.5}$ at 750 °C with the literature data

	Li_2MnO_3		$LiMn_2O_4$	
	Literature data[33]	Le Bail fit data	Literature data[34]	Le Bail fit data
Sp. Gr.	*C*2/*c*		*Fd*-3*m*	
a ()Å	4.921(6)	4.9272(1)	8.2211(4)	8.2193(2)
b ()Å	8.526(3)	8.5250(1)		
c ()Å	9.606(5)	9.6139(2)		
β (deg.)	99.47(5)	99.542(1)		

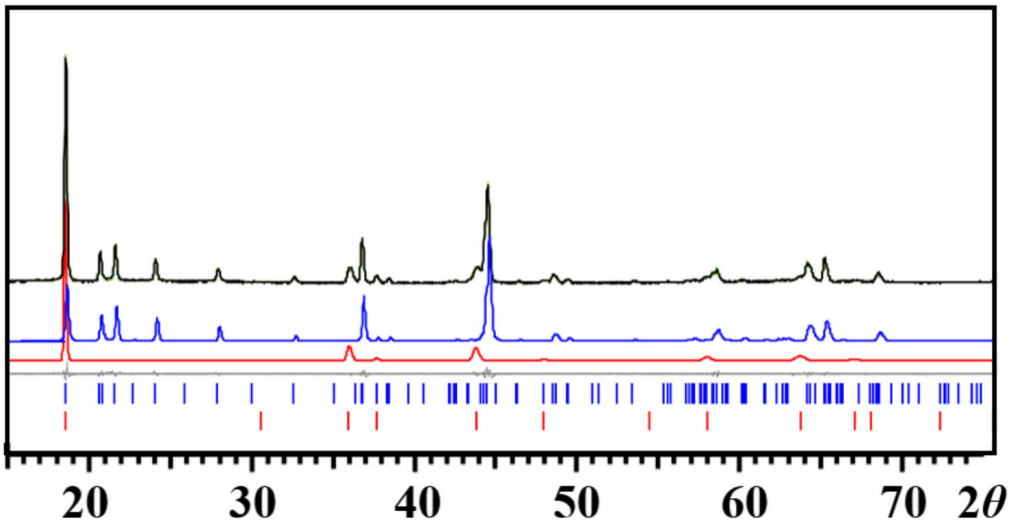

Figure 10. Powder X-ray diffraction pattern of the residue obtained by heating $Li_{1.5}Mn_{1.5}O_{3.5}$ at 750 °C in the air and the Le Bail fit. Black and green curves are experimental and calculated overlaid patterns. Blue and red curves are calculated as single peak patterns for Li_2MnO_3 and $LiMn_2O_4$, respectively. The theoretical peak positions are shown at the bottom, and the grey line is the difference curve.

In our previous works with low-temperature synthesis of manganates, we detected a number of new (unknown) phases[38,39]. Many of those compounds appeared to be complex oxyfluorides. However, in every instance, these phases were observed in mixtures, making it nearly impossible to determine their structure and composition, let alone to measure their properties. Perhaps the clearest example was the preparation of a Pb-Mn oxide[39] with a todorokite structure that was still obtained as a mixture, albeit with a known phase.

We report here a new Li-Mn oxide phase and define it through a thorough investigation of its composition, structure, Mn oxidation state, and oxygen content as the Li-rich, oxygen-deficient spinel, $Li_{1.5}Mn_{1.5}O_{3.5}$. We show that this phase disproportionates stoichiometrically upon heating into the thermodynamically stable phases Li_2MnO_3 and $LiMn_2O_4$.

This work represents a rare example of using single-source precursors for making previously unknown, metastable, low-temperature phases. Particularly noteworthy is the successful isolation of the phase in its pure form. This achievement was made possible by employing a well-defined molecular precursor with specific ligands that facilitate low-temperature decomposition. Prior to this work, we designed several single-source precursors in the Li-Mn system with 1:1 and 1:2[26] metal ratios, but those exhibited relatively high decomposition temperatures, not resulting in new phases.

We believe that other unknown or unusual metastable phases can still be discovered in the Li-Mn-O system, particularly those with high Li content. The key to isolating these phases lies in using specific metal ratios, low-temperature synthetic approaches, and the right decomposition conditions to effectively and precisely control the oxygen content.

DECLARATIONS

Authors' contributions

Writing: Han, H.; Zhang, Y.; Dikarev, E. V.; Abakumov, A. M.
Experimentation: Han, H.; Zhang, Y.; Chang, J.
Materials characterization: Zhang, Y.; Han, H.; Filatov, A. S.; Wei, Z.; Batuk, M.; Hadermann, J.; Chang, J.
Manuscript review: Dikarev, E. V.; Abakumov, A. M.; Hadermann, J.

Availability of data and materials

The data are available upon request from the authors.

Financial support and sponsorship

Financial support from the National Science Foundation is gratefully acknowledged for grants CHE-1955585 and CHE-2400091 (E.V.D.). NSF's ChemMatCARS, Sector 15 at the Advanced Photon Source (APS), Argonne National Laboratory (ANL), is supported by the Divisions of Chemistry (CHE) and Materials Research (DMR), National Science Foundation, under grant number CHE-1834750. This research used resources from the Advanced Photon Source, a U.S. Department of Energy (DOE) Office of Science user facility operated for the DOE Office of Science by Argonne National Laboratory under Contract No. DE-AC02-06CH11357. H.H. acknowledges the Fundamental Research Funds for the Central Universities (22120240204) and the National Natural Science Foundation of China (22101205).

Conflicts of interest

All authors declared no conflicts of interest.

Ethical approval and consent to participate

Not applicable.

Consent for publication

Not applicable.

Copyright

© The Author(s) 2025.

REFERENCES

1. Gopalakrishnan, J. Chimie douce approaches to the synthesis of metastable oxide materials. *Chem. Mater.* **1995**, *7*, 1265-75. DOI
2. Stein, A.; Keller, S. W.; Mallouk, T. E. Turning down the heat: design and mechanism in solid-state synthesis. *Science* **1993**, *259*, 1558-64. DOI PubMed
3. Manthiram, A.; Kim, J. Low Temperature synthesis of insertion oxides for lithium batteries. *Chem. Mater.* **1998**, *10*, 2895-909. DOI
4. Elfimov, I. S.; Anisimov, V. I.; Sawatzky, G. A. Orbital ordering, Jahn-Teller distortion, and anomalous X-Ray scattering in manganates. *Phys. Rev. Lett.* **1999**, *82*, 4264-7. DOI
5. Kim, Y. M.; He, J.; Biegalski, M. D.; et al. Probing oxygen vacancy concentration and homogeneity in solid-oxide fuel-cell cathode materials on the subunit-cell level. *Nat. Mater.* **2012**, *11*, 888-94. DOI
6. Hao, X.; Lin, X.; Lu, W.; Bartlett, B. M. Oxygen vacancies lead to loss of domain order, particle fracture, and rapid capacity fade in lithium manganospinel ($LiMn_2O_4$) batteries. *ACS. Appl. Mater. Interfaces.* **2014**, *6*, 10849-57. DOI
7. Alonso, J. A.; Martínez-Lope, M. J.; Casais, M. T.; Fernández-Díaz, M. T. Evolution of the Jahn-Teller distortion of MnO_6 octahedra in $RMnO_3$ perovskites (R = Pr, Nd, Dy, Tb, Ho, Er, Y): a neutron diffraction study. *Inorg. Chem.* **2000**, *39*, 917-23. DOI

8. Lufaso, M. W.; Woodward, P. M. Jahn-Teller distortions, cation ordering and octahedral tilting in perovskites. *Acta. Crystallogr. B.* **2004**, *60*, 10-20. DOI PubMed
9. Lutz, H. D.; Becker, W.; Müller, B.; Jung, M. Raman single crystal studies of spinel type MCr_2S_4(M=Mn, Fe, Co, Zn, Cd), MIn_2S_4(M= Mn, Fe, Co, Ni), $MnCr_{2-2-x}In_{2x}S_4$ and $Co_{1-x}Cd_xCr_2S_4$†. *J. Raman. Spectroscopy.* **1989**, *20*, 99-103. DOI
10. Lutz, H.; Müller, B.; Steiner, H. Lattice vibration spectra. LIX. Single crystal infrared and Raman studies of spinel type oxides. *J. Solid. State. Chem.* **1991**, *90*, 54-60. DOI
11. Sun, J. Z.; Gallagher, W. J.; Duncombe, P. R.; et al. Observation of large low-field magnetoresistance in trilayer perpendicular transport devices made using doped manganate perovskites. *Appl. Phys. Lett.* **1996**, *69*, 3266-8. DOI
12. Bi, Z.; Guo, X. Solidification for solid-state lithium batteries with high energy density and long cycle life. *Energy. Mater.* **2022**, *2*, 200011. DOI
13. Lu, J.; Zhan, C.; Wu, T.; et al. Effectively suppressing dissolution of manganese from spinel lithium manganate via a nanoscale surface-doping approach. *Nat. Commun.* **2014**, *5*, 5693. DOI
14. Heng, Y.; Gu, Z.; Guo, J.; Yang, X.; Zhao, X.; Wu, X. Research progress on the surface/interface modification of high-voltage lithium oxide cathode materials. *Energy. Mater.* **2022**, 2. DOI
15. Komaba, S. Hydrothermal synthesis of high crystalline orthorhombic $LiMnO_2$ as a cathode material for Li-ion batteries. *Solid. State. Ionics.* **2002**, *152-153*, 311-8. DOI
16. Thackeray, M. M. Manganese oxides for lithium batteries. *Prog. Solid. State. Chem.* **1997**, *25*, 1-71. DOI
17. Freire, M.; Kosova, N. V.; Jordy, C.; et al. A new active Li-Mn-O compound for high energy density Li-ion batteries. *Nat. Mater.* **2016**, *15*, 173-7. DOI
18. Ammundsen, B.; Paulsen, J. Novel lithium-ion cathode materials based on layered manganese oxides. *Adv. Mater.* **2001**, *13*, 943-56. DOI
19. Yao, Z.; Kim, S.; He, J.; Hegde, V. I.; Wolverton, C. Interplay of cation and anion redox in $Li_4Mn_2O_5$ cathode material and prediction of improved $Li_4(Mn,M)_2O_5$ electrodes for Li-ion batteries. *Sci. Adv.* **2018**, *4*, eaao6754. DOI
20. Chitrakar, R.; Kanoh, H.; Miyai, Y.; Ooi, K. A new type of manganese oxide ($MnO_2{\cdot}0.5H_2O$) derived from $Li_{1.6}Mn_{1.6}O_4$ and its lithium ion-sieve properties. *Chem. Mater.* **2000**, *12*, 3151-7. DOI
21. 21. Xiao JL, Sun SY, Wang J, Li P, Yu J. Synthesis and adsorption properties of Li1.6Mn1.6O4 spinel. Ind Eng Chem Res 2013;52:11967-73. DOI
22. Sun, S.; Xiao, J.; Wang, J.; Song, X.; Yu, J. Synthesis and adsorption properties of $Li_{1.6}Mn_{1.6}O_4$ by a combination of redox precipitation and solid-phase reaction. *Ind. Eng. Chem. Res.* **2014**, *53*, 15517-21. DOI
23. Han, H.; Wei, Z.; Barry, M. C.; Filatov, A. S.; Dikarev, E. V. Heterometallic molecular precursors for a lithium-iron oxide material: synthesis, solid state structure, solution and gas-phase behaviour, and thermal decomposition. *Dalton. Trans.* **2017**, *46*, 5644-9. DOI PubMed
24. Han, H.; Zhou, Z.; Carozza, J. C.; et al. From lithium to sodium: design of heterometallic molecular precursors for the $NaMO_2$ cathode materials†. *Chem. Commun.* **2019**, *55*, 7243-6. DOI
25. Han, H.; Wei, Z.; Barry, M. C.; et al. A three body problem: a genuine heterotrimetallic molecule vs. a mixture of two parent heterobimetallic molecules. *Chem. Sci.* **2018**, *9*, 4736-45. DOI
26. Wei, Z.; Han, H.; Filatov, A. S.; Dikarev, E. V. Changing the bridging connectivity pattern within a heterometallic assembly: design of single-source precursors with discrete molecular structures. *Chem. Sci.* **2014**, *5*, 813-8. DOI
27. Gross, J. H. Direct analysis in real time-a critical review on DART-MS. *Anal. Bioanal. Chem.* **2014**, *406*, 63-80. DOI PubMed
28. Hosono, E.; Kudo, T.; Honma, I.; Matsuda, H.; Zhou, H. Synthesis of single crystalline spinel $LiMn_2O_4$ nanowires for a lithium ion battery with high power density. *Nano. Lett.* **2009**, *9*, 1045-51. DOI PubMed
29. Takada, T.; Hayakawa, H.; Akiba, E. Preparation and crystal structure refinement of $Li_4Mn_5O_{12}$ by the rietveld method. *J. Solid. State. Chem.* **1995**, *115*, 420-6. DOI
30. Kawai, H.; Nagata, M.; Kageyama, H.; Tukamoto, H.; West, A. R. 5 V lithium cathodes based on spinel solid solutions $Li_2Co_{1+X}Mn_{3-X}O_8$: -1≤X≤1. *Electrochim. Acta.* **1999**, *45*, 315-27. DOI
31. Takada, T.; Akiba, E.; Izumi, F.; Chakoumakos, B. C. Structure refinement of $Li_4Mn_5O_{12}$with neutron and X-Ray powder diffraction data. *J. Solid. State. Chem.* **1997**, *130*, 74-80. DOI
32. Boulineau, A.; Croguennec, L.; Delmas, C.; Weill, F. Thermal stability of Li_2MnO_3: from localized defects to the spinel phase. *Dalton. Trans.* **2012**, *41*, 1574-81. DOI
33. Riou, A.; Lecerf, A.; Gerault, Y.; Cudennec, Y. Etude structurale de Li_2MnO_3. *Mater. Res. Bull.* **1992**, *27*, 269-75. DOI
34. Berg, H. Neutron diffraction study of electrochemically delithiated $LiMn_2O_4$ spinel. *Solid. State. Ionics.* **1999**, *126*, 227-34. DOI
35. Pei, Y.; Chen, Q.; Xiao, Y.; et al. Understanding the phase transitions in spinel-layered-rock salt system: criterion for the rational design of LLO/spinel nanocomposites. *Nano. Energy.* **2017**, *40*, 566-75. DOI
36. Takada, T.; Hayakawa, H.; Akiba, E.; Izumi, F.; Chakoumakos, B. C. Novel synthesis process and structure refinements of $Li_4Mn_5O_{12}$ for rechargeable lithium batteries. *J. Power. Sources.* **1997**, *68*, 613-7. DOI
37. Croguennec, L. Electrochemical behavior of orthorhombic $LiMnO_2$: influence of the grain size and cationic disorder. *Solid. State. Ionics.* **1996**, *89*, 127-37. DOI
38. Lieberman, C. M.; Filatov, A. S.; Wei, Z.; Rogachev, A. Y.; Abakumov, A. M.; Dikarev, E. V. Mixed-valent, heteroleptic homometallic diketonates as templates for the design of volatile heterometallic precursors. *Chem. Sci.* **2015**, *6*, 2835-42. DOI

PubMed PMC

39. Zhang, H.; Yang, J. H.; Shpanchenko, R. V.; et al. New class of single-source precursors for the synthesis of main group-transition metal oxides: heterobimetallic Pb-Mn β-diketonates. *Inorg. Chem.* **2009**, *48*, 8480-8. DOI